A 71GHz RF Energy Harvesting Tag with 8% Efficiency for Wireless Temperature Sensors in 65nm CMOS

Hao Gao, Marion K. Matters-Kammerer, Pieter Harpe, Dusan Milosevic, Ulf Johannsen

Arthur van Roermund, Peter Baltus

Department of Electrical Engineering, Eindhoven University of Technology, The Netherlands

***Abstract* — This paper presents the first monolithically integrated RF-power harvesting 71 GHz wireless temperature sensor node in 65nm CMOS technology, containing a monopole antenna, a 71 GHz RF power harvesting unit with storage capacitor array, an End-of-Burst monitor, a temperature sensor and an ultra-low-power transmitter at 79 GHz. At 71 GHz, the RF to DC converter achieves a power conversion efficiency of 8% for 5 dBm input power.**

***Index Terms* — RF Energy Harvesting, Tag, Efficiency, wireless sensor, CMOS.**

I. Introduction

Future wireless sensor networks require reliable, battery-less, miniaturized, low-cost sensor nodes with ultra-low power consumption. Remote RF-powering provides a reliable, wireless source of power for such monolithically integrated sensor nodes [1]. Mm-wave RF-energy harvesting and data transfer will enable CMOS on-chip antenna integration. Moreover, an important advantage of mm-wave wireless energy transfer is the higher received power level that can be achieved through a much narrower and highly directive beam [2] than would be created by a similar-sized phased array at lower frequencies. Therefore, going to mm-wave operation is a crucial step towards successful wireless sensor networks [3]. Such monolithically integrated nodes require no additional packaging or maintenance. The maximum range of this type of nodes critically depends on the efficiency of the RF energy harvesting with on-chip rectifiers, on generating sufficient energy for activating the node and on minimizing the required transmitter (Tx) power. Recent publications [4][5] demonstrate RFID tags either working at lower frequencies, from HF (13.56 MHz) to UHF frequencies (860 MHz to 2.45 GHz), or with limited efficiency at mm-wave frequency (1.2% at 45 GHz with 2 dBm input power [6]). Also, the on-chip transmitter for this application has different requirements than the more typical W-band transmitters such as [7]. For example, the transmit power should be much lower, while maintaining a good efficiency because of limited power that can be harvested.

This paper presents the first monolithically-integrated power-harvesting 71 GHz wireless temperature sensing node, consisting of an on-chip $\lambda/4$ monopole antenna, an on-chip 71 GHz RF power harvesting unit with storage capacitor, an End-of-Burst monitor, a temperature sensor and an ultra-low-power transmitter at 79 GHz. The on-chip rectifier achieves 8% efficient power harvesting at 5 dBm input power. At the same power level, the efficiency is 6.6 times higher than in [6] and the input sensitivity is comparable to [6] despite the significantly higher operating frequency.

This paper is organized as follows. In section II, the system architecture and block diagram of the wireless node is described. In section III, the analysis of the mm-wave rectifier is presented and the three-stage inductor-peaked rectifier architecture is proposed. In section IV, the design of the wireless sensor node integrated in 65 nm CMOS technology is provided. In section V, the measured results of the implemented sensor node are shown. The conclusions are drawn in section VI.

II. System Architecture

Figure 1 shows a block diagram of the 71 GHz wireless node. The RF power is transmitted from the base station to the sensor node. The antenna receives the RF power, and feeds it to the input of the RF energy harvesting unit. The RF-DC converter rectifies the incoming RF power and the harvested energy is stored on the on-chip storage

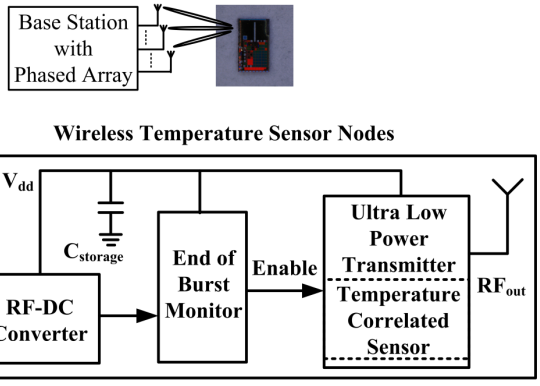

Figure 1: Block diagram of the RF energy harvesting wireless temperature sensor.

capacitor. This energy is used later to power the Tx. The End-of-Burst monitor detects when the incoming power signal ends and turns the Tx part on. Then the Tx transmits a signal back around 79 GHz. The exact value of the transmit frequency depends on temperature. By measuring this Tx frequency, the base station can monitor the environmental temperature of the sensor node.

III. Three-Stage Inductor-Peaked Rectifier

Figure 2 shows the three-stage inductor-peaked rectifier, which provides the supply voltage for the active circuits. Mm-wave RF energy harvesting efficiency is improved by inductor-peaked diodes, threshold voltage modulation, and a low-pass output filter.

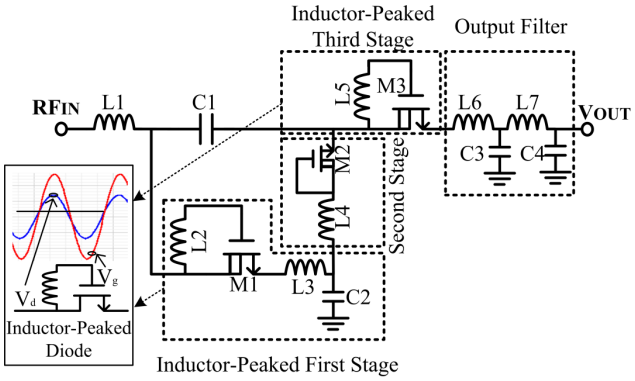

Figure 2: Schematic of the three-stage inductor-peaked rectifier.

In the chosen CMOS technology, Schottky diodes are not a standard library component, and the diodes in the rectifiers are formed by diode connected transistors. The sensitivity is mainly limited by the RF input voltage swing and the threshold voltage V_{th}. The efficiency is limited by V_{th}, the on-resistance R_{on} and parasitic capacitors of the transistor. When the transistor is turned on, R_{on} determines the insertion loss at low frequencies. At mm-wave operating frequency, the insertion loss will increase due to the capacitive coupling of the signal through the parasitic capacitances of the transistor to the substrate. In the OFF state, at low working frequencies, the off-resistance R_{off} determines the isolation. R_{off} is typically more than one hundred k , leading to a very good isolation at low frequencies. However, at mm-wave frequencies, isolation becomes worse due to transistor parasitic capacitances. The RF signal, coupled through C_{gs} to the output, will discharge the storage capacitor in the negative phase, which will lower the output voltage and decrease the efficiency. To increase the efficiency, this paper applies an improved inductor-peaked diode stage, in which the drain and gate are connected through an inductor. Because of the resonance of the inductor and C_{gs} of the transistor, the voltage swing at the gate is larger than at the drain, which decreases R_{on} because of the increased voltage (V_{gs}-V_{th}). M_1, L_2 is the inductor-peaked first stage. Taking into account the interconnect parasitics and striving for a minimum area, the second stage is formed by the diode connected transistor M_2 and the inductor L_4. M_3, L_5 form the inductor-peaked third stage. In Figure 2, L_1 is the input series inductor matching stage. There are several general methods of impedance matching, such as transformer matching, shunt inductor matching and series inductor matching [8]. Compared with the other solutions, the series inductor matching can take advantage of the voltage-boosting effect at the input of the rectifier due to the Q-factor of the inductor, which will also improve the sensitivity and efficiency of the rectifier. The threshold voltage of the transistor is the bottleneck of the rectifier, because it is related directly to the sensitivity and the efficiency [9]. There are several threshold voltage modulation methods that are used in the HF/UHF range [10]. At mm-wave frequency, in order to make the design robust to the parasitic capacitors, the self-threshold voltage modulation is proposed and implemented by connecting the pwell of the nMOS to the drain, which lowers the turn-on voltage of the nMOS. L_3 together with C_2 form a filter for the first stage output DC voltage. L_6, L_7, C_3 and C_4 form the low-pass output filter. The output filter is used to remove the RF signal from the DC path, which prevents the coupled RF signal from discharging the storage capacitor and increases the efficiency.

IV. Wireless Sensor Node

Figure 3 shows the simplified schematic of the full wireless node. The DC voltage is generated by the three-stage inductor-peaked rectifier, and it is stored in the on-

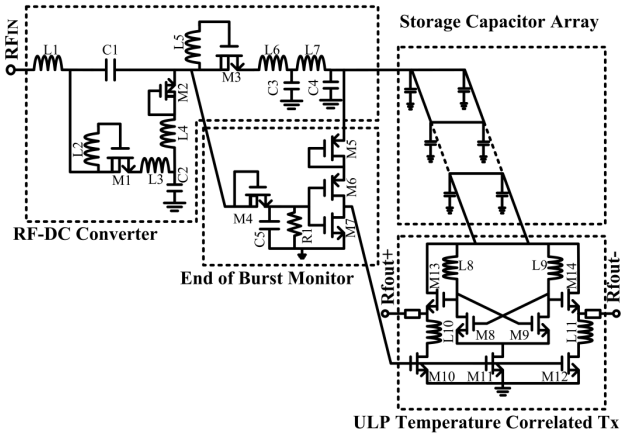

Figure 3: Schematic of the tag, including the RF-DC converter, End of Burst Monitor, the storage capacitor and the ultra-low power (ULP) temperature correlated transmission stage (TX).

chip capacitor array.

In order to increase the capacitor density, a MoM capacitor was integrated below the MiM capacitor. The capacitor array is connected such that it has a low series resistance. The End-of-Burst monitor is formed by an inverter (M_5, M_6, M_7) and a small rectifier (M_4, C_5) with a small resistor load (R_1). The input of the monitor is attached to the input of the third stage of the rectifier.

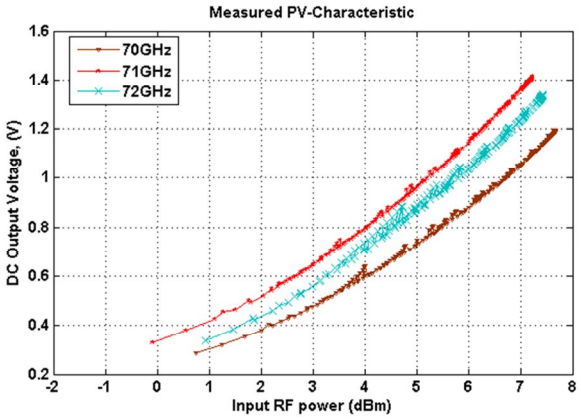

Figure 4: Measured rectifier output voltage as a function of RF input power.

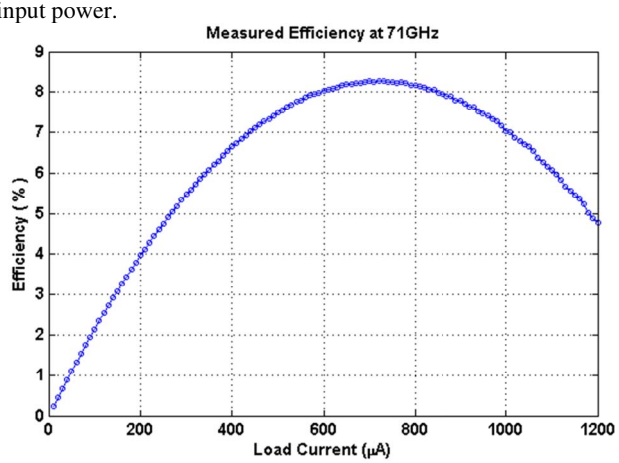

Figure 5: Measured rectifier efficiency with load current at 71 GHz with 5 dBm input power.

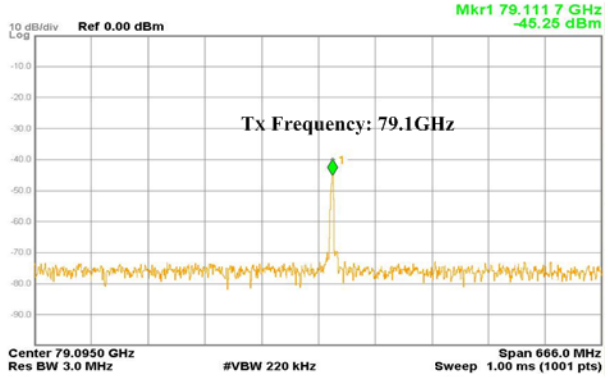

Figure 6: Measured Tx frequency.

After the RF power burst ends, the End-of-Burst monitor generates the enable signal to the ultra-low power transmit stage (Tx), consisting of a VCO and output buffer. The 79 GHz oscillator generates the output burst when the enable signal is high.

V. Measurement Result

The chip is measured with on-wafer RF and DC probes. Figure 4 shows the measured sensitivity of the three stage inductor-peaked rectifier. With 5 dBm input power at 71 GHz to activate the tag, the output voltage is 1 V with 1 M load. Figure 5 shows the measured efficiency of the three stage inductor-peaked rectifier. The maximum efficiency at 71 GHz is 8% for a 700 μA current load. The

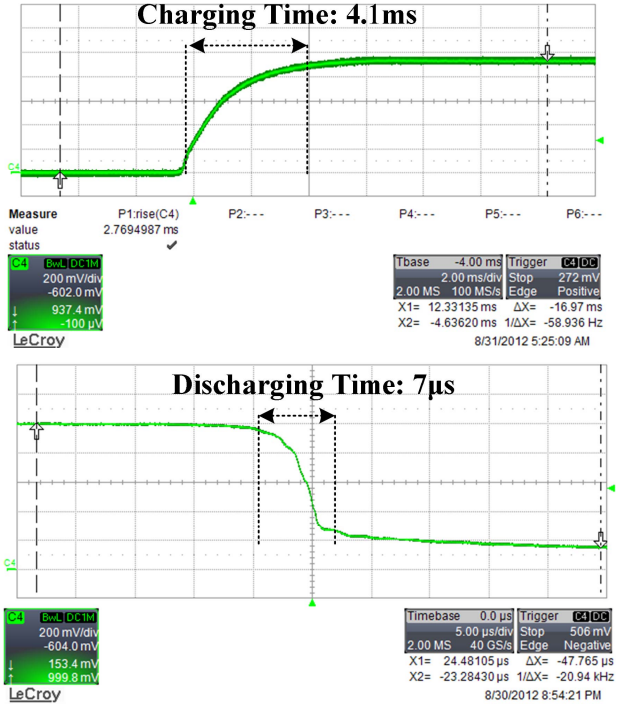

Figure 7: Measured time domain tag charging and discharging with 5 dBm input RF power.

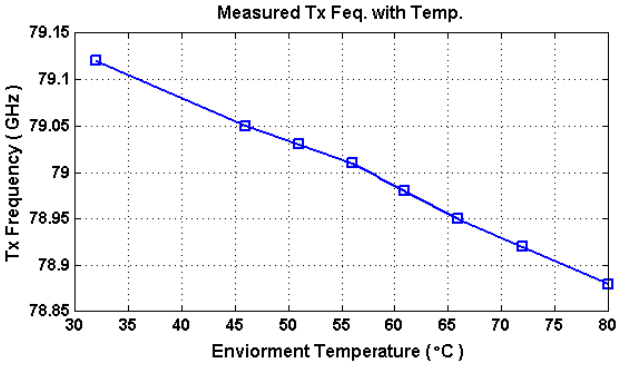

Figure 8: Measured Tx frequency relationship to environment temperature.

minimum required supply voltage for the oscillator to start oscillation is 670 mV and the Tx current consumption is 4 mA, and the Tx frequency is 79.1 GHz as shown in Figure 6. Figure 7 shows the charging and discharging of the tag. With 5 dBm input power at 71 GHz, the system is charged to 937 mV in 4.1 ms. When the RF input power signal ends, the tag fully discharges in 7 µs, as shown in Figure 7. During discharging, the oscillator frequency is related to ambient temperature. From 32 ℃ to 80 ℃, it shows a reasonably linear behavior between 79.12 GHz to 78.88 GHz with slope k=-22 MHz/℃ (Figure 8).

The 71 GHz energy harvesting tag was implemented in 65nm CMOS and occupies 1.16×0.94 mm^2 chip area, (Figure 9).

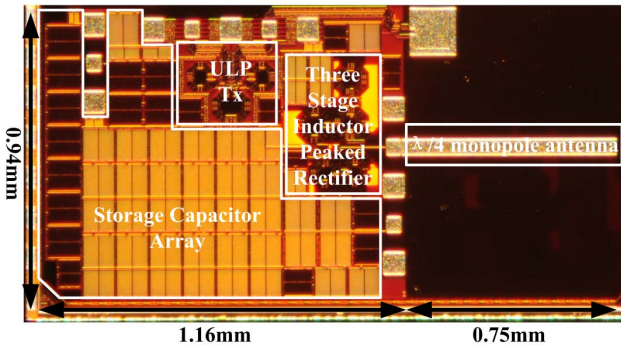

Figure 9: Die micrograph of the 71 GHz RF energy harvesting temperature sensing tag in 65nm CMOS.

VI. Conclusion

Table 1 summarizes the measured performance of the three-stage inductor-peaked rectifier and sensor node. Compared to state-of-the-art alternatives, the presented design operates at a far higher frequency (Rx: 71 GHz; Tx: 79.1 GHz) and it is fully integrated, while also providing the best efficiency (8%) at 5 dBm input power. By detecting the frequency that has been transmitted by the node, the base station can determine the node temperature.

	ISSCC 2011 [4]	ISSCC 2012 [5]	JSSC 2010 [6]	This work
Technology	130nm	90nm	90nm	65nm
Area	0.95mm^2	1.54mm2	1.235mm^2	1.09mm^2
Area with Antenna	Not available	Not available	Not available	1.79mm^2
RF Harvesting Frequency	860MHz to 2.45GHz	902 to 928MHz	45GHz	70 to 72GHz
Rectifier Efficiency	Not available	Not available	1.2% @ 45GHz	8% @ 71GHz
Power to wake up the node	-10dBm	-15dBm	2dBm @ 45GHz	5dBm @ 71GHz
Tx Frequency	860MHz to 2.45GHz	2.405 to 2.475GHz	60GHz	79.1GHz

Table 1: Performance summary and comparison with prior art.

Acknowledgement

This work has been funded by Technology Foundation STW, the Netherlands. Project name: PREMISS, number: 10544. The authors wish to acknowledge Philips for the financial support for the tape-out.

References

[1] F. Kocer and M. P. Flynn, "A New Transponder Architecture with On-Chip ADC for Long-Range," IEEE Journal of Solid-State Circuits, vol. 41, no. 5, pp. 1142-1148, May , 2006.

[2] Y, Yu, P. Baltus, A. van Roermund, E. van der Heijden, M. Collados, C.Vaucher, "A 60GHz digitally controlled RF-beamforming receiver front-end in 65nm CMOS" Radio Frequency Integrated Circuits Symposium, 2009. RFIC 2009. IEEE, pp.211-214, 7-9 June 2009.

[3] Y. Wu, Jean-Paul Linnartz, H. Gao, P. Baltus and J.W.M. Bergmans, "System study of a 60 GHz wireless-powered monolithic sensor system," Information, Communications and Signal Processing (ICICS) 2011 8th International Conference on , pp.1-5, 13-16 Dec. 2011.

[4] H. Reinisch, M. Wiessflecker, S. Gruber, H. Unterassinger, G. Hofer, M. Klamminger, W. Pribyl, G. Holweg, "A 7.9 W Remotely Powered Addressed Sensor Node Using EPC HF and UHF RFID Technology with -10.3dBm Sensitivity," Solid-State Circuits Conference Digest of Technical Papers (ISSCC), 2011 IEEE International, pp.454-456, 20-24 Feb. 2011.

[5] G. Papotto, F. Carrara, A. Finocchiaro, G. Palmisano, "A 90nm CMOS 5Mb/s Crystal-Less RF Transceiver for RF-Powered WSN Nodes," Solid-State Circuits Conference Digest of Technical Papers (ISSCC), 2012 IEEE International, pp.452-454, 19-23 Feb. 2012.

[6] S. Pellerano, J. Alvarado, Y. Palaskas, "A mm-Wave Power-Harvesting RFID Tag in 90nm CMOS," Solid-State Circuits, IEEE Journal of, vol.45, no.8, pp.1627-1637, Aug. 2010.

[7] X. Li, P. Baltus, P. van Zeijl, D. Milosevic, A. van Roermund, "A 70GHz 10.2mW Self-Demodulator for OOK Modulation in 65-nm CMOS Technology," Custom Integrated Circuits Conference (CICC), 2010 IEEE, pp.1-4, 19-22 Sept. 2010.

[8] R. Barnett, J. Liu, S. Lazar, "A RF to DC Voltage Conversion Model for Multi-Stage Rectifiers in UHF RFID Transponders", Solid-State Circuits, IEEE Journal of, vol.44, no.2, pp.354-370, Feb. 2009.

[9] H. Gao, et al., "2.4GHz Energy Harvesting for Wireless Sensor Network", Wireless Sensors and Sensor Networks (WiSNet), 2011 IEEE Topical Conference on, pp.57-60, 16-19 Jan. 2011.

[10] K. Kotani, T. Ito, "High Efficinecy CMOS Rectifier Circuit with Self-Vth-Cancellation and Power Regulation Functions for UHF RFIDs", Solid-State Circuits Conference, 2007. ASSCC '07. IEEE Asian, pp.119-122, 12-14 Nov. 2007.